NANO LETTERS

pubs.acs.org/NanoLett Letter

Possible Topological Hall Effect above Room Temperature in Layered $Cr_{1.2}Te_2$ Ferromagnet

Meng Huang, Lei Gao, Ying Zhang, Xunyong Lei, Guojing Hu, Junxiang Xiang, Hualing Zeng, Xuewen Fu, Zengming Zhang, Guozhi Chai, Yong Peng, Yalin Lu, Haifeng Du, Gong Chen, Jiadong Zang, and Bin Xiang*

Cite This: https://doi.org/10.1021/acs.nanolett.1c00493 Read Online

ACCESS | Metrics & More | Article Recommendations | Supporting Information

ABSTRACT: Topological Hall effect (THE) has been used as a powerful tool to unlock spin chirality in novel magnetic materials. Recent focus has been widely paid to THE and possible chiral spin textures in two-dimensional (2D) layered magnetic materials. However, the room-temperature THE has been barely reported in 2D materials, which hinders its practical applications in 2D spintronics. In this paper, we report a possible THE signal featuring antisymmetric peaks in a wide temperature window up to 320 K in $Cr_{1.2}Te_2$, a new quasi-2D ferromagnetic material. The temperature, thickness, and magnetic field dependences of the THE lead to potential spin chirality origin that is associated with the spin canting under external magnetic fields. Our work holds promise for practical applications in future chiral spin-based vdW spintronic devices.

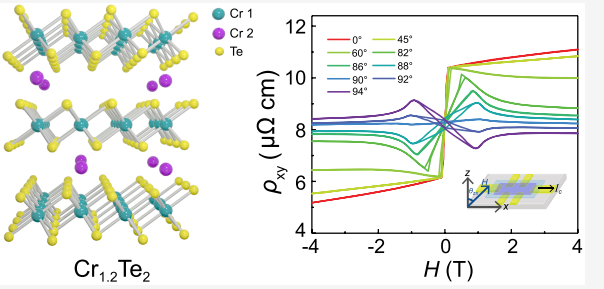

KEYWORDS: *topological Hall effect, spin chirality, room-temperature ferromagnet, layered structure, spintronics*

Spin chirality possessing novel topological textures in real space (for example, skyrmions and skyrmion bubbles)[1−9] have attracted intensive research interest due to their promising spintronics applications.[10,11] A scheme to electrically detect the spin chirality is a crucial issue in those applications. Understanding electron transport coupled with chiral magnetism is a fundamental subject in condensed matter physics. Transport signature indeed provides a powerful tool to detect spin chirality.[12,13] When an electron moves through the system, in real space, the spin chirality can endow the electron with a phase factor, and result in an additional transverse voltage in anomalous Hall effect, dubbed topological Hall effect (THE).[14−16] The antisymmetric spike observed in the anomalous Hall resistivity at low external magnetic field has been considered as the hallmark of THE. Because of its dependence on spin chirality, THE is considered to be instrumental in the electric detection of chiral spin textures.[17,18]

The topological Hall effect has been widely reported in chiral B20 magnets, such as MnSi,[19] MnGe,[20] double-exchange ferromagnet CrO_2,[21] the kagome magnet Fe_3Sn_2,[22] the heterostructure of TmIG/Pt,[12] the frustrated magnet $Nd_2Mo_2O_7$ with a pyrochlore lattice,[23] and $PdCrO_2$ with a triangular lattice.[24] It has also been discovered in achiral itinerant magnets with competing spin interactions.[18,25] Recently, the THE has been reported in two-dimensional (2D) ferromagnetic materials, such as chiral skyrmion induced THE in Fe_3GeTe_2.[26−28] Such findings open the door to the fundamental study of chiral spin textures in 2D magnets and their potential device applications. However, room-temperature THE in 2D layered materials has barely been reported, which hinders the practical applications in future 2D spintronics. In this paper, we report a pronounced topological Hall effect within a large temperature window up to 320 K in a quai-2D ferromagnet of Cr-intercalated $CrTe_2$ ($Cr_{1.2}Te_2$).

$Cr_{1.2}Te_2$ was synthesized by an oxidation process of $KCrTe_2$ with iodine in acetonitrile (details in Methods). Figure 1a demonstrates the self-intercalation of Cr atoms into the structure of $CrTe_2$. Figure 1b,c shows that the additional Cr atoms fill the van der Waals gaps with fractional site occupations between the $CrTe_2$ layers, forming the structure of $Cr_{1.2}Te_2$. The chemical content of the as-synthesized $Cr_{1.2}Te_2$ was quantified to be a mole ratio of 1.2:2 by inductively coupled plasma-atomic emission spectrometry (Table S2, Supporting Information). X-ray diffraction characterization (Figure 1d) reveals that the as-synthesized $Cr_{1.2}Te_2$ has the same crystal structure as $CrTe_2$, containing the space group $P\bar{3}m1$ and exhibiting a crystal structure distinguished

Received: February 4, 2021
Revised: May 11, 2021

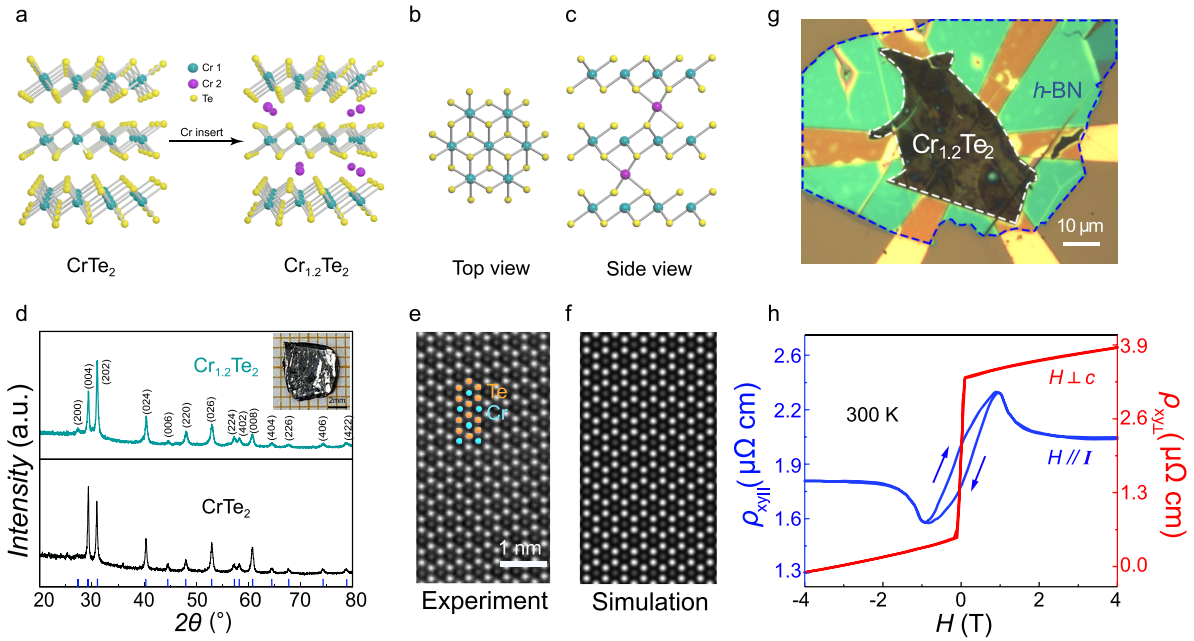

Figure 1. (a) Schematic illustration of $Cr_{1.2}Te_2$ structure formation by intercalating Cr atoms into van der Waals gaps of $CrTe_2$. Cr fractional occupation in purple color. Atomic structure of $Cr_{1.2}Te_2$ in top (b) and side (c) views. (d) Powder X-ray diffraction results for $Cr_{1.2}Te_2$ and $CrTe_2$, showing identical XRD patterns. Simulation of $Cr_{1.2}Te_2$ XRD in blue curve. Inset: Optical image of as-synthesized $Cr_{1.2}Te_2$ crystal. (e) HRSTEM image of as-synthesized $Cr_{1.2}Te_2$ and its corresponding simulated HRSTEM in (f). (g) Optical picture of 59 nm thick $Cr_{1.2}Te_2$-based Hall bar device encapsulated by a layer of h-BN. (h) Raw data of Hall resistivity $\rho_{xy\parallel}$ under the external field almost parallel to the probe current and $\rho_{xy\perp}$ under $H\|c$ at 300 K.

from other reported telluride compounds (Figure S1, Supporting Information) such as Cr_2Te_3, Cr_3Te_4, Cr_3Te_5, Cr_4Te_5, and Cr_5Te_8.[29−32] The high-resolution scanning transmission electron microscopy (HRSTEM) image of the as-synthesized $Cr_{1.2}Te_2$ (Figure 1e) and its corresponding simulation (Figure 1f) further confirm that the crystal structure duplicates that of the reported $CrTe_2$.[33]

The $M-T$ curves (Figure S2a, Supporting Information) show a Curie temperature of ∼320 K in as-synthesized $Cr_{1.2}Te_2$. The $M-H$ curve (Figure S2b, Supporting Information) reveals a perpendicular magnetic anisotropy (PMA) in the $Cr_{1.2}Te_2$ at 300 K in contrast to easy-plane anisotropy in $CrTe_2$,[33,34] with a saturation magnetic moment of ∼0.94 μ_B/Cr atom at 300 K. Our calculated effective magnetic anisotropy K_{eff} with a value of 7.4×10^4 J/m^3 > 0, further confirms the perpendicular magnetic anisotropy in $Cr_{1.2}Te_2$ at 300 K (Note S1, Supporting Information). The small coercivity of ∼20 Oe indicates a soft ferromagnet of as-synthesized $Cr_{1.2}Te_2$ (Figure S2b, Supporting Information). At low temperatures, the as-grown $Cr_{1.2}Te_2$ exhibits in-plane magnetic anisotropy, confirmed by the calculated effective magnetic anisotropy of K_{eff} < 0, while the $Cr_{1.2}Te_2$ magnetization easy axis can be rotated from in-plane to out-of-plane direction when the temperature is higher than 140 K (Table S3, Supporting Information).

The formation process of the $Cr_{1.2}Te_2$ structure is the same as that of $Cr_{1+x}Te_2$,[35] $Cr_{1.234}Te_{1.75}Se_{0.25}$[36] and $Cr_{1.3}Te_{1.75}Se_{0.25}$[36] by a self-intercalation of Cr atoms into the van der Waals gap of $CrTe_2$, maintaining the same structure as the host $CrTe_2$. The intercalated Cr atoms in the van der Waals gap occupy the octahedral vacancies being covalently bonded with the host of $CrTe_2$[37] in which the crystal dimension is in analogy to quasi-2D materials of $Fe_{0.29}TaS_2$[38] and $Co_{1/3}NbS_2$.[39] The fractional occupation in the van der Waals gap provides available sites for a different amount of intercalated Cr atoms. In $Cr_{1.2}Te_2$, the vacancy occupancy rate is ∼20% and the average strength of a covalent bond between the adjacent layers is weaker than intralayer interactions. Thus, $Cr_{1.2}Te_2$ can be mechanically exfoliated into thin flakes with a thickness down to ∼5 nm (Figure S3, Supporting Information).

Fractional stoichiometry in $Cr_{1.2}Te_2$ leads to disordered distribution of Cr atoms and random neighboring distances. Therefore, the Ruderman−Kittel−Kasuya−Yosida (RKKY) interactions[40−42] could play a significant role in spin exchange in the intercalated layer and competing spin interactions become possible. This is indeed indicated by our susceptibility data. Fitting result on the temperature dependence of inverse magnetic susceptibility by Curie−Weiss law (Figure S2c, Supporting Information) reveals the transition temperature from ferromagnetic to paramagnetic phase is 308 K lower than the Curie temperature of 320 K, supporting the presence of competing interactions in this material. It has been reported in Gd_2PdSi_3[18] and $Gd_3Ru_4Al_{12}$[25] that competing RKKY interaction in triangle lattice can induce the skyrmion lattice as superposition of three equal lateral spin helices. The RKKY interaction or other competing interactions may induce the spin canting in $Cr_{1.2}Te_2$ crystal. The saturation magnetization in $Cr_{1.2}Te_2$ is ∼2.25 μ_B/Cr atom at 3 K, which is much smaller than the expected saturation magnetic moment of 3 μ_B/Cr atom calculated from an ionic model[43] and effective paramagnetic moment 4−4.5 μ_B/Cr atom.[44−46] This discrepancy confirmed that $Cr_{1.2}Te_2$ exhibits spin canting.

To reveal the presence of spin chirality, the Hall measurement was employed. Utilizing a dry transfer method, we fabricated a Hall effect device based on a mechanically exfoliated $Cr_{1.2}Te_2$ flake as shown in Figure 1g. When an external magnetic field is applied parallel to the c-axis, the Hall

https://doi.org/10.1021/acs.nanolett.1c00493
Nano Lett. XXXX, XXX, XXX−XXX

resistivity $\rho_{xy\perp}$ exhibits nonlinear behavior, which indicates ferromagnetic order-induced anomalous Hall effect (Note S2, Supporting Information).[47,48] When the magnetic field is almost parallel with the probe current in $a-b$ plane with a polar angle of 89°, an antisymmetric peak feature is observed even in the raw data of Hall resistivity ρ_{xy} (Figure 1h), which shows a hint of the topological Hall effect. However, in principle we cannot exclude the reported mechanisms of the PMA-induced abnormal peak in the angular-dependent Hall effect[49] regarding the antisymmetric peaks observed in Hall resistivity.

To further probe the THE behavior in the Hall resistivity, we rotate the magnetic field from perpendicular to parallel while probing current in the $a-b$ plane. Figure 2a shows the raw data of Hall resistivity ρ_{xy} at different field-rotation angles θ_{zx} between the external magnetic field and the normal of the sample $a-b$ plane. When θ_{zx} is higher than 45°, the anomaly in the Hall resistivity ρ_{xy} exhibits a cusplike feature with a maximum value of ~ 10 $\mu\Omega$·cm in the low field, indicating an angular dependence of topological Hall effect. A clear hump structure is also observed in the magnetoresistance (MR) curves in Figure 2b at the same field-rotation angle θ_{zx} (see Note S6, Supporting Information for more discussion).

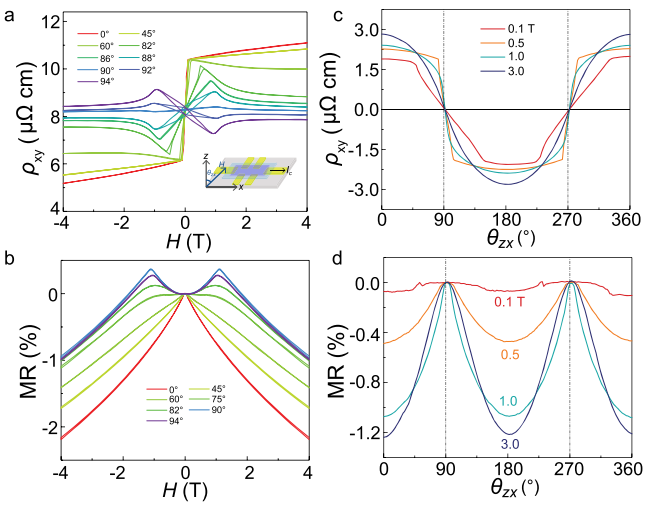

Figure 2. (a) Raw data of Hall resistivity ρ_{xy} at 300 K under different field orientation angles θ_{zx}. Inset: θ_{zx} definition. (b) Magnetic field dependence of MR curves at 300 K with different field-orientation angles θ_{zx}. (c) Angular dependence of ρ_{xy} at 300 K under the different field strengths 0.1, 0.5, 1, and 3 T. (d) Angular dependence of MR at 300 K under the different field strengths of 0.1, 0.5, 1, and 3 T.

Figure 2c shows the angular dependence of the Hall resistivity ρ_{xy} under different magnetic fields. It is interesting that the Hall resistivity ρ_{xy} becomes almost a constant at low fields of 0.1, 0.5, and 1 T when the field orientation is off the $a-b$ plane, while ρ_{xy} follows a cos θ_{zx} relation at a higher field of 3 T (Figure S4, Supporting Information). This anisotropic ρ_{xy} reflects that the expected additional transverse voltage contributes to the Hall resistivity by the parallel component of the low external magnetic field. MR's angular dependence shows 2-fold symmetry (peaks at 91.2° and 272°) in Figure 2d with anisotropy of −1.2% at 3 T.

The temperature dependence of the Hall resistivity shows a clear difference between magnetic fields applied along the c-axis and $a-b$ plane. When the magnetic field is parallel to the c-axis, measurements in Figure 3a show that the antisymmetric peak feature can be observed at 3 and 10 K. This could be a result of non-negligible contribution from MR due to the presence of a spin glass feature, which is supported by the deviation between field cooling (FC) and zero field cooling (ZFC) (Figure S2a, Supporting Information). The antisymmetric peak in anomalous Hall resistivity ρ_{AHE} vanishes at a temperature of 30 K when the glass feature is suppressed. In contrast, under the magnetic field parallel to the probe current in $a-b$ plane, the antisymmetric peak in Hall resistivity $\rho_{xy\parallel}$ is absent at low temperature, but gradually emerges at 30 K and above (Figure 3b) and persists up to 320 K (Figure 3c). As discussed above, the PMA behavior in $Cr_{1.2}Te_2$ only appears when the temperature is above 140 K (Table S3, Supporting Information). Therefore, the observed antisymmetric peaks in Hall resistivity should not be attributed to the simple PMA-

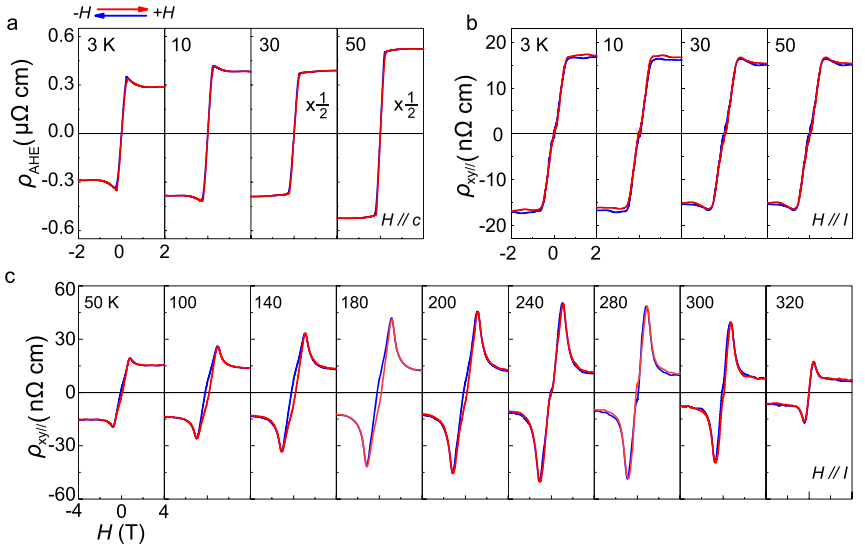

Figure 3. (a) Magnetic-field dependence of anomalous Hall resistivity ρ_{AHE} of the $Cr_{1.2}Te_2$ flake at different temperatures under $H\|c$. (b,c) Magnetic field dependence of $\rho_{xy\|}$ extracted by $[\rho_{xy\|}(+H) - \rho_{xy\|}(-H)]/2$ at temperatures from 50 to 320 K under the external field almost parallel to the probe current. Note that the polar angle of the external field $\theta_{zx} \approx 89°$.

https://doi.org/10.1021/acs.nanolett.1c00493
Nano Lett. XXXX, XXX, XXX−XXX

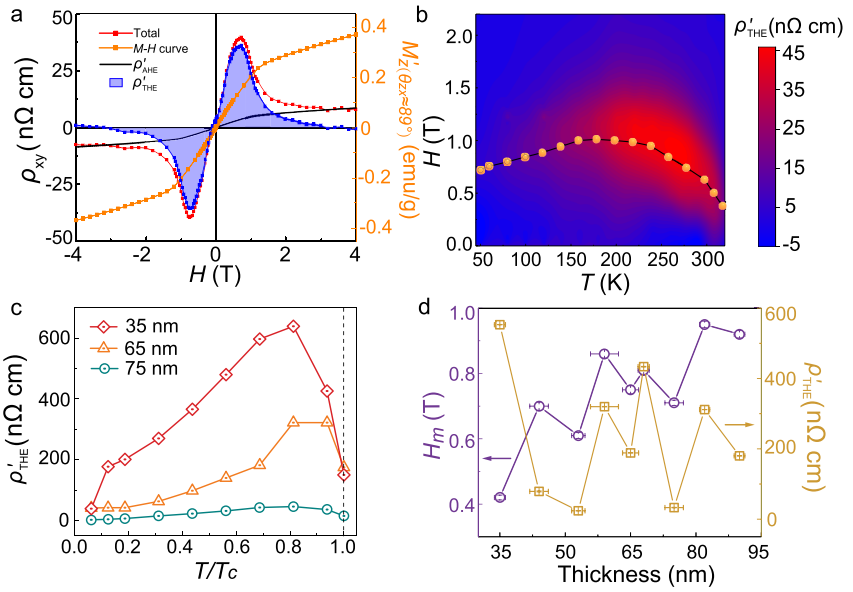

Figure 4. (a) Magnetic field H dependence of ρ_{xy}, $M'_{z(\theta_{zx}\approx 89°)}$, ρ'_{AHE}, and ρ'_{THE} at 300 K for 68 nm $Cr_{1.2}Te_2$ flake. θ_{zx} is the angle between the c-axis and the external field H. The ρ'_{THE} was obtained by subtracting the partial AHE contribution ρ'_{AHE} from ρ_{xy}. (b) Color map of ρ'_{THE} as a function of magnetic field H and temperature T. (c) Maximum values of ρ'_{THE} as a function of temperature for $Cr_{1.2}Te_2$ flakes with different thicknesses. (d) Thickness dependence of maximum values of ρ'_{THE} and the corresponding field H_m at 300 K.

induced abnormal Hall resistivity. The data are well reproduced in different thickness of $Cr_{1.2}Te_2$ flakes (Figure S5, Supporting Information).

Between 30 and 320 K, the spin glass feature almost vanishes, and furthermore, the peaks are clearly invisible in the raw data. Figure 3 shows no sign changes in our $Cr_{1.2}Te_2$ anomalous Hall resistivity when the temperature is increased from 3 to 320 K. The angular dependence of $M-H$ measurement shows isotropic magnetization in the $a-b$ plane with no different coercive field observed in the loop (Figure S6, Supporting Information), revealing no specially separated magnetic regions in our $Cr_{1.2}Te_2$. Therefore, we can exclude the contribution from the opposite-sign anomalous Hall effect (AHE) of the separated magnetic regions to our topological Hall resistivity.[50]

Because of the equipment limitation, it is hard to precisely determine the component (M_z) of the $Cr_{1.2}Te_2$ magnetization (M) along the z-axis direction when we rotate the external magnetic field. Therefore, we are unable to thoroughly extract the AHE signal and precisely obtain the THE magnitude ρ_{THE}. However, the PMA property in $Cr_{1.2}Te_2$ provides a chance to roughly estimate the THE contribution by utilizing M'_z to subtract the partial AHE contribution ρ'_{AHE} (Note S4, Supporting Information). When the rotated external magnetic field is below the saturated field, the estimated THE contribution (ρ'_{THE}) is slightly larger than the actual THE ρ_{THE} because of $M'_z \leq M_z$ causing an underestimation of the AHE contribution. Figure 4a shows that the magnitude term of the antisymmetric peak ρ'_{THE} is obtained by subtracting the partial AHE contribution ρ'_{AHE} from the total Hall resistivity ρ_{xy}. Figure 4b shows the mapping of the extracted ρ'_{THE} as a function of the external magnetic field and temperature, also showing the magnetic field dependence of the antisymmetric peak location in THE. In other $Cr_{1.2}Te_2$ flakes with different thicknesses, we also observe the similar topological Hall effect (Figure S7, Supporting Information). Figure 4c reveals that the antisymmetric peaks can be obtained at temperatures up to 320 K and exhibits a maximum value of ρ'_{THE} at 260 K, remaining a relatively large value around T_c. Figure 4d shows the nonmonotonic thickness dependence of ρ'_{THE} in different $Cr_{1.2}Te_2$ devices. Although ρ'_{THE} is the roughly estimated THE contribution, the temperature and thickness dependence of ρ'_{THE} still deserve certain attention to reveal the THE evolution and are consistent with the fact that the skyrmion phase locates around T_c in B20 chiral magnet.[2,51,52] Thermal fluctuations can further enhance the THE even at elevated temperatures.[53] We thus conclude that the thermal fluctuations may be a major driving force behind the topological Hall effect in $Cr_{1.2}Te_2$.

In summary, we report THE over a large temperature window up to 320 K in quasi-2D ferromagnet $Cr_{1.2}Te_2$. The thickness, temperature, and field-orientation dependence of the THE signal reveals the promising appearance of spin chirality. Because of the vdW structure, the easy cleavage enables us to explore the thickness dependence of chiral skyrmion phase transition and the thinner sample enhances the stability of skyrmion over a wide range of temperature and magnetic field, facilitating the realization of skyrmion-based devices.

METHODS

$Cr_{1.2}Te_2$ and $CrTe_2$ Single Crystal Synthesis. The $Cr_{1.2}Te_2$ single crystal was prepared by oxidation of $KCr_{1.2}Te_2$ with iodine in acetonitrile. The single crystal of $KCr_{1.2}Te_2$ was grown by mixing K, Cr, and Te in a glovebox. Then the mixture was placed in a quartz tube and sealed in vacuum. Then the mixture was heated up to 900 °C in 24 h and kept at this temperature for 7 days. After returning to room temperature and considering $KCr_{1.2}Te_2$ was sensitive to air and water, the growth tube was opened in a glovebox to avoid degradation. Then as-grown single crystal $KCr_{1.2}Te_2$ was then added into solutions of iodine in acetonitrile to remove the K ions through deintercalation reaction. The product was washed by acetonitrile several times, then filtered and dried in vacuum. Finally, we obtained the $Cr_{1.2}Te_2$. We also synthesized the $CrTe_2$ single crystal with similar methods. Magnetization

https://doi.org/10.1021/acs.nanolett.1c00493
Nano Lett. XXXX, XXX, XXX−XXX

characterizations of $Cr_{1.2}Te_2$ and $CrTe_2$ single crystals were carried out by a vibrating sample magnetometer (MPMS 3, Quantum Design) under external magnetic field along the $a-b$ plane and c-axis.

ICP-AES Measurements. The element molar ratio of as-synthesized $Cr_{1.2}Te_2$ crystal was determined by inductively coupled plasma atomic emission spectrometry (ICP-AES, Optima 7300 DV). A certain amount of $Cr_{1.2}Te_2$ single crystal was dissolved in aqua regia (mixture of nitric acid and hydrochloric acid) and then the solution was diluted by adding DI water to make the element concentration below 80 ppm.

Exfoliated flake-based Hall Bar Device Fabrication. The standard Hall bar devices were fabricated on a SiO_2 (300 nm)/ Si (500 μm) substrate using ultraviolet lithography (SUSS MBA6), followed by metal deposition (Ti/Au: 8 nm/ 25 nm) and a lift-off process. Then the exfoliated $Cr_{1.2}Te_2$ flakes were transferred onto the prepatterned Ti/Au Hall bars through our homemade transfer station in a glovebox. Because $Cr_{1.2}Te_2$ flakes are sensitive to air, they was encapsulated by a layer of hexagonal boron nitride (h-BN) on the device top to prevent degradation during further characterizations. The thicknesses of $Cr_{1.2}Te_2$ flakes were measured using an atomic force microscope (Bruker, Dimension Icon) in tapping mode.

Transport Measurements. Transport measurements for exfoliated $Cr_{1.2}Te_2$ flakes were performed in physical property measurement system (Quantum Design, PPMS-9T). The longitudinal resistance and Hall resistance were measured using a standard five-terminal method with an alternate current of 500 uA in the $a-b$ plane.

■ ASSOCIATED CONTENT

Supporting Information

The Supporting Information is available free of charge at https://pubs.acs.org/doi/10.1021/acs.nanolett.1c00493.

> Additional data about effective magnetic anisotropy (K_{eff}), anomalous Hall effect, THE extracted from Hall resistivity, temperature dependence of magnetic anisotropy, angle dependence of MR curve and THE; powder XRD pattern of $Cr_{1.2}Te_2$, $M-T$ curves and $M-H$ curves at 300 K; optical image and atomic force morphology image of exfoliated $Cr_{1.2}Te_2$ flake; $M-H$ curves at 300 and 3 K at different field-orientation angle θ; raw data of ρ_{xy} at different $Cr_{1.2}Te_2$ thickness when H is almost parallel to the probe current; anomalous Hall effect data with $H\|c$-axis; magnetic field dependence of ρ_{xy} and MR under different field-tilting angle θ_{zy} at 300 K; magnetic field dependence of ρ_{xy} at 300 K under different field-tilting angle θ_{zx}; magnetic field dependence of in-plane ρ_{xy} and MR under different field-tilting angle θ_{xy} at 300 K; ICP-AES results (PDF)

■ AUTHOR INFORMATION

Corresponding Author

Bin Xiang − *Hefei National Laboratory for Physical Sciences at the Microscale, Department of Materials Science and Engineering, CAS Key Lab of Materials for Energy Conversion and Anhui Laboratory of Advanced Photon Science and Technology, University of Science and Technology of China, Hefei, Anhui 230026, China;* orcid.org/0000-0001-8254-8640; Email: binxiang@ustc.edu.cn

Authors

Meng Huang − *Hefei National Laboratory for Physical Sciences at the Microscale, Department of Materials Science and Engineering, CAS Key Lab of Materials for Energy Conversion, University of Science and Technology of China, Hefei, Anhui 230026, China;* orcid.org/0000-0001-6493-8223

Lei Gao − *Key Laboratory of Magnetism and Magnetic Materials of the Ministry of Education, Lanzhou University, Lanzhou 730000, P.R. China*

Ying Zhang − *Hefei National Laboratory for Physical Sciences at the Microscale, Department of Materials Science and Engineering, CAS Key Lab of Materials for Energy Conversion, University of Science and Technology of China, Hefei, Anhui 230026, China*

Xunyong Lei − *Hefei National Laboratory for Physical Sciences at the Microscale, Department of Materials Science and Engineering, CAS Key Lab of Materials for Energy Conversion, University of Science and Technology of China, Hefei, Anhui 230026, China*

Guojing Hu − *Hefei National Laboratory for Physical Sciences at the Microscale, Department of Materials Science and Engineering, CAS Key Lab of Materials for Energy Conversion, University of Science and Technology of China, Hefei, Anhui 230026, China*

Junxiang Xiang − *Hefei National Laboratory for Physical Sciences at the Microscale, Department of Materials Science and Engineering, CAS Key Lab of Materials for Energy Conversion, University of Science and Technology of China, Hefei, Anhui 230026, China*

Hualing Zeng − *Hefei National Laboratory for Physical Sciences at the Microscale, Department of Materials Science and Engineering, CAS Key Lab of Materials for Energy Conversion, University of Science and Technology of China, Hefei, Anhui 230026, China;* orcid.org/0000-0001-5869-9553

Xuewen Fu − *School of Physics, Nankai University, Tianjin 300071, China;* orcid.org/0000-0001-6116-4680

Zengming Zhang − *The Center for Physical Experiments, University of Science and Technology of China, Hefei, Anhui 230026, China;* orcid.org/0000-0001-8245-9955

Guozhi Chai − *Key Laboratory of Magnetism and Magnetic Materials of the Ministry of Education, Lanzhou University, Lanzhou 730000, P.R. China*

Yong Peng − *Key Laboratory of Magnetism and Magnetic Materials of the Ministry of Education, Lanzhou University, Lanzhou 730000, P.R. China;* orcid.org/0000-0002-6980-4694

Yalin Lu − *Hefei National Laboratory for Physical Sciences at the Microscale, Department of Materials Science and Engineering, CAS Key Lab of Materials for Energy Conversion and Anhui Laboratory of Advanced Photon Science and Technology, University of Science and Technology of China, Hefei, Anhui 230026, China*

Haifeng Du − *High Magnetic Field Laboratory, Chinese Academy of Science (CAS), Hefei, Anhui Province 230031,, China*

Gong Chen − *Physics Department, Georgetown University, Washington, DC 20057, United States;* orcid.org/0000-0002-5102-7487

Jiadong Zang − *Department of Physics and Materials Science Program, University of New Hampshire, Durham, New Hampshire 03824, United States*

https://doi.org/10.1021/acs.nanolett.1c00493
Nano Lett. XXXX, XXX, XXX−XXX

Complete contact information is available at:
https://pubs.acs.org/10.1021/acs.nanolett.1c00493

Notes

The authors declare no competing financial interest.

■ ACKNOWLEDGMENTS

This work was supported by the National Key Research and Development Program of China (2017YFA0402902). J.Z. was supported by U.S. Department of Energy, Office of Science, Basic Energy Sciences (Grant DE-SC0020221). The Fundamental Research Funds for the Central Universities (Grant WK2030020032 and WK3510000013). The Anhui Initiative in Quantum Information Technologies (Grant AHY170000). Work at GU was supported by the U.S. NSF (DMR-2005108). This research was partially carried out at the USTC Center for Micro and Nanoscale Research and Fabrication.

■ REFERENCES

(1) Gao, S.; Rosales, H. D.; Albarracin, F. G. A.; Tsurkan, V.; Kaur, G.; Fennell, T.; Steffens, P.; Boehm, M.; Cermak, P.; Schneidewind, A.; Ressouche, E.; Cabra, D. C.; Ruegg, C.; Zaharko, O. Fractional antiferromagnetic skyrmion lattice induced by anisotropic couplings. *Nature* **2020**, *586*, 37−41.

(2) Yu, X. Z.; Onose, Y.; Kanazawa, N.; Park, J. H.; Han, J. H.; Matsui, Y.; Nagaosa, N.; Tokura, Y. Real-space observation of a two-dimensional skyrmion crystal. *Nature* **2010**, *465*, 901−904.

(3) Kezsmarki, I.; Bordacs, S.; Milde, P.; Neuber, E.; Eng, L. M.; White, J. S.; Ronnow, H. M.; Dewhurst, C. D.; Mochizuki, M.; Yanai, K.; Nakamura, H.; Ehlers, D.; Tsurkan, V.; Loidl, A. Neel-type skyrmion lattice with confined orientation in the polar magnetic semiconductor GaV_4S_8. *Nat. Mater.* **2015**, *14*, 1116−1122.

(4) Khanh, N. D.; Nakajima, T.; Yu, X. Z.; Gao, S.; Shibata, K.; Hirschberger, M.; Yamasaki, Y.; Sagayama, H.; Nakao, H.; Peng, L. C.; Nakajima, K.; Takagi, R.; Arima, T. H.; Tokura, Y.; Seki, S. Nanometric square skyrmion lattice in a centrosymmetric tetragonal magnet. *Nat. Nanotechnol.* **2020**, *15*, 444−449.

(5) Yu, X.; Kanazawa, N.; Onose, Y.; Kimoto, K.; Zhang, W.; Ishiwata, S.; Matsui, Y.; Tokura, Y. Near room-temperature formation of a skyrmion crystal in thin-films of the helimagnet FeGe. *Nat. Mater.* **2011**, *10*, 106−109.

(6) Zhou, Y. Magnetic skyrmions: intriguing physics and new spintronic device concepts. *Nati. Sci. Rev.* **2019**, *6*, 210−212.

(7) Yu, X.; Koshibae, W.; Tokunaga, Y.; Shibata, K.; Taguchi, Y.; Nagaosa, N.; Tokura, Y. Transformation between Meron and skyrmion topological spin textures in a chiral magnet. *Nature* **2018**, *564*, 95−98.

(8) Fert, A.; Reyren, N.; Cros, V. Magnetic skyrmions: advances in physics and potential applications. *Nature Reviews Materials* **2017**, *2*, 17031.

(9) Han, J. H.; Zang, J.; Yang, Z.; Park, J.-H.; Nagaosa, N. Skyrmion lattice in a two-dimensional chiral magnet. *Phys. Rev. B: Condens. Matter Mater. Phys.* **2010**, *82*, No. 094429.

(10) Zhang, X.; Zhou, Y.; Mee Song, K.; Park, T.-E.; Xia, J.; Ezawa, M.; Liu, X.; Zhao, W.; Zhao, G.; Woo, S. Skyrmion-electronics: writing, deleting, reading and processing magnetic skyrmions toward spintronic applications. *J. Phys.: Condens. Matter* **2020**, *32*, 143001.

(11) Back, C.; Cros, V.; Ebert, H.; Everschor-Sitte, K.; Fert, A.; Garst, M.; Ma, T.; Mankovsky, S.; Monchesky, T. L.; Mostovoy, M.; Nagaosa, N.; Parkin, S. S. P.; Pfleiderer, C.; Reyren, N.; Rosch, A.; Taguchi, Y.; Tokura, Y.; von Bergmann, K.; Zang, J. The 2020 skyrmionics roadmap. *J. Phys. D: Appl. Phys.* **2020**, *53*, 363001.

(12) Shao, Q. M.; Liu, Y. W.; Yu, G. Q.; Kim, S. K.; Che, X. Y.; Tang, C.; He, Q. L.; Tserkovnyak, Y.; Shit, J.; Wang, K. L. Topological Hall effect at above room temperature in heterostructures composed of a magnetic insulator and a heavy metal. *Nat. Electron.* **2019**, *2*, 182−186.

(13) Wang, L. F.; Feng, Q. Y.; Kim, Y.; Kim, R.; Lee, K. H.; Pollard, S. D.; Shin, Y. J.; Zhou, H. B.; Peng, W.; Lee, D.; Meng, W. J.; Yang, H.; Han, J. H.; Kim, M.; Lu, Q. Y.; Noh, T. W. Ferroelectrically tunable magnetic skyrmions in ultrathin oxide heterostructures. *Nat. Mater.* **2018**, *17*, 1087−1094.

(14) Bruno, P.; Dugaev, V. K.; Taillefumier, M. Topological Hall effect and Berry phase in magnetic nanostructures. *Phys. Rev. Lett.* **2004**, *93*, No. 096806.

(15) Jiang, W. J.; Chen, G.; Liu, K.; Zang, J. D.; te Velthuis, S. G. E.; Hoffmann, A. Skyrmions in magnetic multilayers. *Phys. Rep.* **2017**, *704*, 1−49.

(16) Vistoli, L.; Wang, W. B.; Sander, A.; Zhu, Q. X.; Casals, B.; Cichelero, R.; Barthelemy, A.; Fusil, S.; Herranz, G.; Valencia, S.; Abrudan, R.; Weschke, E.; Nakazawa, K.; Kohno, H.; Santamaria, J.; Wu, W. D.; Garcia, V.; Bibes, M. Giant topological Hall effect in correlated oxide thin films. *Nat. Phys.* **2019**, *15*, 104−104.

(17) Wang, W.; Daniels, M. W.; Liao, Z.; Zhao, Y.; Wang, J.; Koster, G.; Rijnders, G.; Chang, C.-Z.; Xiao, D.; Wu, W. Spin chirality fluctuation in two-dimensional ferromagnets with perpendicular magnetic anisotropy. *Nat. Mater.* **2019**, *18*, 1054−1059.

(18) Kurumaji, T.; Nakajima, T.; Hirschberger, M.; Kikkawa, A.; Yamasaki, Y.; Sagayama, H.; Nakao, H.; Taguchi, Y.; Arima, T.; Tokura, Y. Skyrmion lattice with a giant topological Hall effect in a frustrated triangular-lattice magnet. *Science* **2019**, *365*, 914−918.

(19) Lee, M.; Kang, W.; Onose, Y.; Tokura, Y.; Ong, N. P. Unusual Hall Effect Anomaly in MnSi under Pressure. *Phys. Rev. Lett.* **2009**, *102*, 186601.

(20) Kanazawa, N.; Onose, Y.; Arima, T.; Okuyama, D.; Ohoyama, K.; Wakimoto, S.; Kakurai, K.; Ishiwata, S.; Tokura, Y. Large Topological Hall Effect in a Short-Period Helimagnet MnGe. *Phys. Rev. Lett.* **2011**, *106*, 156603.

(21) Yanagihara, H.; Salamon, M. B. Skyrmion strings and the anomalous Hall effect in CrO_2. *Phys. Rev. Lett.* **2002**, *89*, 187201.

(22) Li, H.; Ding, B.; Chen, J.; Li, Z.; Hou, Z.; Liu, E.; Zhang, H.; Xi, X.; Wu, G.; Wang, W. Large topological Hall effect in a geometrically frustrated kagome magnet Fe_3Sn_2. *Appl. Phys. Lett.* **2019**, *114*, 192408.

(23) Taguchi, Y.; Oohara, Y.; Yoshizawa, H.; Nagaosa, N.; Tokura, Y. Spin chirality, Berry phase, and anomalous Hall effect in a frustrated ferromagnet. *Science* **2001**, *291*, 2573−2576.

(24) Takatsu, H.; Yonezawa, S.; Fujimoto, S.; Maeno, Y. Unconventional Anomalous Hall Effect in the Metallic Triangular-Lattice Magnet $PdCrO_2$. *Phys. Rev. Lett.* **2010**, *105*, 137201.

(25) Hirschberger, M.; Nakajima, T.; Gao, S.; Peng, L.; Kikkawa, A.; Kurumaji, T.; Kriener, M.; Yamasaki, Y.; Sagayama, H.; Nakao, H.; Ohishi, K.; Kakurai, K.; Taguchi, Y.; Yu, X.; Arima, T.-h.; Tokura, Y. Skyrmion phase and competing magnetic orders on a breathing kagomé lattice. *Nat. Commun.* **2019**, *10*, 5831.

(26) Wang, Y.; Xian, C.; Wang, J.; Liu, B.; Ling, L.; Zhang, L.; Cao, L.; Qu, Z.; Xiong, Y. Anisotropic anomalous Hall effect in triangular itinerant ferromagnet Fe_3GeTe_2. *Phys. Rev. B: Condens. Matter Mater. Phys.* **2017**, *96*, 134428.

(27) You, Y.; Gong, Y.; Li, H.; Li, Z.; Zhu, M.; Tang, J.; Liu, E.; Yao, Y.; Xu, G.; Xu, F.; Wang, W. Angular dependence of the topological Hall effect in the uniaxial van der Waals ferromagnet Fe_3GeTe_2. *Phys. Rev. B: Condens. Matter Mater. Phys.* **2019**, *100*, 134441.

(28) Park, T.-E.; Peng, L.; Liang, J.; Hallal, A.; Yasin, F. S.; Zhang, X.; Song, K. M.; Kim, S. J.; Kim, K.; Weigand, M.; Schütz, G.; Finizio, S.; Raabe, J.; Garcia, K.; Xia, J.; Zhou, Y.; Ezawa, M.; Liu, X.; Chang, J.; Koo, H. C.; et al. Néel-type skyrmions and their current-induced motion in van der Waals ferromagnet-based heterostructures. *Phys. Rev. B: Condens. Matter Mater. Phys.* **2021**, *103*, 104410.

(29) Hamasaki, T.; Hashimoto, T.; Yamaguchi, Y.; Watanabe, H. Neutron-Diffraction Study of Cr_2Te_3 Single-Crystal. *Solid State Commun.* **1975**, *16*, 895−897.

(30) Yamaguchi, M.; Hashimoto, T. Magnetic Properties of Cr_3Te_4 in Ferromagnetic Region. *J. Phys. Soc. Jpn.* **1972**, *32*, 635−638.

(31) Zhang, L.-Z.; Zhang, A.-L.; He, X.-D.; Ben, X.-W.; Xiao, Q.-L.; Lu, W.-L.; Chen, F.; Feng, Z.; Cao, S.; Zhang, J.; Ge, J.-Y. Critical behavior and magnetocaloric effect of the quasi-two-dimensional

https://doi.org/10.1021/acs.nanolett.1c00493
Nano Lett. XXXX, XXX, XXX−XXX

room-temperature ferromagnet Cr_4Te_5. *Phys. Rev. B: Condens. Matter Mater. Phys.* **2020**, *101*, 214413.
(32) Wang, Y.; Yan, J.; Li, J.; Wang, S.; Song, M.; Song, J.; Li, Z.; Chen, K.; Qin, Y.; Ling, L.; Du, H.; Cao, L.; Luo, X.; Xiong, Y.; Sun, Y. Magnetic anisotropy and topological Hall effect in the trigonal chromium tellurides Cr_5Te_8. *Phys. Rev. B: Condens. Matter Mater. Phys.* **2019**, *100*, No. 024434.
(33) Sun, X.; Li, W.; Wang, X.; Sui, Q.; Zhang, T.; Wang, Z.; Liu, L.; Li, D.; Feng, S.; Zhong, S.; Wang, H.; Bouchiat, V.; Nunez Regueiro, M.; Rougemaille, N.; Coraux, J.; Purbawati, A.; Hadj-Azzem, A.; Wang, Z.; Dong, B.; Wu, X.; et al. Room temperature ferromagnetism in ultra-thin van der Waals crystals of 1T-$CrTe_2$. *Nano Res.* **2020**, *13*, 3358−3363.
(34) Freitas, D. C.; Weht, R.; Sulpice, A.; Remenyi, G.; Strobel, P.; Gay, F.; Marcus, J.; Núñez-Regueiro, M. Ferromagnetism in layered metastable 1T-$CrTe_2$. *J. Phys.: Condens. Matter* **2015**, *27*, 176002.
(35) Fujisawa, Y.; Pardo-Almanza, M.; Garland, J.; Yamagami, K.; Zhu, X.; Chen, X.; Araki, K.; Takeda, T.; Kobayashi, M.; Takeda, Y.; Hsu, C. H.; Chuang, F. C.; Laskowski, R.; Khoo, K. H.; Soumyanarayanan, A.; Okada, Y. Tailoring magnetism in self-intercalated $Cr_{1+\delta}Te_2$ epitaxial films. *Phys. Rev. Mater.* **2020**, *4*, 114001.
(36) Lotgering, F.; Gorter, E. Solid solutions between ferromagnetic and antiferromagnetic compounds with NiAs structure. *J. Phys. Chem. Solids* **1957**, *3*, 238−249.
(37) Zhao, X.; Song, P.; Wang, C.; Riis-Jensen, A. C.; Fu, W.; Deng, Y.; Wan, D.; Kang, L.; Ning, S.; Dan, J. Engineering covalently bonded 2D layered materials by self-intercalation. *Nature* **2020**, *581*, 171−177.
(38) Cai, R.; Xing, W.; Zhou, H.; Li, B.; Chen, Y.; Yao, Y.; Ma, Y.; Xie, X. C.; Jia, S.; Han, W. Anomalous Hall effect mechanisms in the quasi-two-dimensional van der Waals ferromagnet $Fe_{0.29}TaS_2$. *Phys. Rev. B: Condens. Matter Mater. Phys.* **2019**, *100*, No. 054430.
(39) Tenasini, G.; Martino, E.; Ubrig, N.; Ghimire, N. J.; Berger, H.; Zaharko, O.; Wu, F.; Mitchell, J. F.; Martin, I.; Forró, L.; Morpurgo, A. F. Giant anomalous Hall effect in quasi-two-dimensional layered antiferromagnet $Co_{1/3}NbS_2$. *Phys. Rev. Research* **2020**, *2*, No. 023051.
(40) Ruderman, M. A.; Kittel, C. Indirect Exchange Coupling of Nuclear Magnetic Moments by Conduction Electrons. *Phys. Rev.* **1954**, *96*, 99−102.
(41) Kasuya, T. A Theory of Metallic Ferro- and Antiferromagnetism on Zener's Model. *Prog. Theor. Phys.* **1956**, *16*, 45−57.
(42) Yosida, K. Magnetic Properties of Cu-Mn Alloys. *Phys. Rev.* **1957**, *106*, 893−898.
(43) Andresen, A. F.; Zeppezauer, E.; Boive, T.; Nordstrom, B.; Branden, C.-I. MAGNETIC STRUCTURE OF Cr_2Te_3, Cr_3Te_4 AND Cr_5Te_6. *Acta Chem. Scand.* **1970**, *24*, 3495−3509.
(44) Hirone, T.; Chiba, S. On the Magnetic Anisotropy of Single Crystal of Chromium Telluride. *J. Phys. Soc. Jpn.* **1960**, *15*, 1991−1994.
(45) Lotgering, F. K.; Gorter, E. W. Solid solutions between ferromagnetic and antiferromagnetic compounds with NiAs structure. *J. Phys. Chem. Solids* **1957**, *3*, 238−249.
(46) Polesya, S.; Mankovsky, S.; Benea, D.; Ebert, H.; Bensch, W. Finite-temperature magnetism of CrTe and CrSe. *J. Phys.: Condens. Matter* **2010**, *22*, 156002.
(47) Nagaosa, N.; Sinova, J.; Onoda, S.; MacDonald, A. H.; Ong, N. P. Anomalous Hall effect. *Rev. Mod. Phys.* **2010**, *82*, 1539−1592.
(48) Kim, K.; Seo, J.; Lee, E.; Ko, K.-T.; Kim, B. S.; Jang, B. G.; Ok, J. M.; Lee, J.; Jo, Y. J.; Kang, W.; Shim, J. H.; Kim, C.; Yeom, H. W.; Il Min, B.; Yang, B.-J.; Kim, J. S. Large anomalous Hall current induced by topological nodal lines in a ferromagnetic van der Waals semimetal. *Nat. Mater.* **2018**, *17*, 794−799.
(49) Tang, J.; Xu, G.; You, Y.; Xu, Z.; Zhang, Z.; Chen, X.; Gong, Y.; Xu, F. Abnormal peak of angular-dependent Hall effect as an indicator for skyrmion in perpendicular magnetic anisotropy system. *Appl. Phys. Lett.* **2020**, *117*, 202402.
(50) Kimbell, G.; Sass, P. M.; Woltjes, B.; Ko, E. K.; Noh, T. W.; Wu, W.; Robinson, J. W. Two-channel anomalous Hall effect in $SrRuO_3$. *Phys. Rev. Mater.* **2020**, *4*, No. 054414.
(51) Yu, X. Z.; Kanazawa, N.; Onose, Y.; Kimoto, K.; Zhang, W. Z.; Ishiwata, S.; Matsui, Y.; Tokura, Y. Near room-temperature formation of a skyrmion crystal in thin-films of the helimagnet FeGe. *Nat. Mater.* **2011**, *10*, 106−109.
(52) Mühlbauer, S.; Binz, B.; Jonietz, F.; Pfleiderer, C.; Rosch, A.; Neubauer, A.; Georgii, R.; Böni, P. Skyrmion Lattice in a Chiral Magnet. *Science* **2009**, *323*, 915.
(53) Hou, W.-T.; Yu, J.-X.; Daly, M.; Zang, J. Thermally driven topology in chiral magnets. *Phys. Rev. B: Condens. Matter Mater. Phys.* **2017**, *96*, 140403.

https://doi.org/10.1021/acs.nanolett.1c00493
Nano Lett. XXXX, XXX, XXX−XXX